Electronic Supplementary Material (ESI) for ChemComm.

Supporting Information

The synergistic effect of Cu-MOF nanoparticles and immunomodulatory agent on SARS-CoV-2 inhibition

Aleksander Ejsmont,[a] Alicja Warowicka,[b,c] Justyna Broniarczyk,[b] and Joanna Goscianska[a,*]

[a]*Adam Mickiewicz University, Faculty of Chemistry, Department of Chemical Technology, Uniwersytetu Poznańskiego 8, 61-614 Poznań, Poland*

[b]*Adam Mickiewicz University, Faculty of Biology, Department of Molecular Virology, Institute of Experimental Biology, Uniwersytetu Poznańskiego 6, 61-614 Poznań, Poland*

[c]*NanoBioMedical Centre, Wszechnicy Piastowskiej 3, 61-614 Poznań, Poland*

*Corresponding author: Tel.: +48-724221607; +48-618291607, E-mail address: asiagosc@amu.edu.pl

TABLE OF CONTENT

1. Experimental Section

1.1. Chemicals

Copper(II) nitrate trihydrate (98%), 1,3,5-benzenetricarboxylic acid (trimesic acid, H_3BTC, 95%), and 1,4-benzenedicarboxylic acid (terephthatlic acid, H_2BDC, 98%) were purchased from Sigma-Aldrich. Sodium formate (HCOONa, 99%) was acquired from Warchem, while hydroxychloroquine sulfate (HCQ, 98%) from Acros Organics. All chemicals were used without further purification.

1.2. Preparation of HKUST-1 nanoparticles

Firstly, copper(II) nitrate trihydrate (9.785 g) and trimesic acid (5.674 g) were dissolved in the mixture of ethanol (324 mL) and distilled water (324 mL). After 1 h, to the continuously stirred mixture, sodium formate (3.673 g) was added, and then all was transferred into the 800 mL Teflon-lined steel autoclave. Subsequently, the synthesis was conducted in the oven by heating the mixture in the closed system at 120 °C for 24 h. The resulting turquoise precipitate was centrifuged, and washed with distilled water and ethanol, followed by drying at 70 °C for 12 h.

1.3. Preparation of Cu-BDC nanoparticles

The second Cu-MOF was prepared similarly to the previous one but with the use of a different linker. In the beginning, copper(II) nitrate trihydrate (9.785 g) and terephthalic acid (4.486 g) were dissolved in the mixture of ethanol (324 mL) and distilled water (324 mL). To the stirred mixture, sodium formate was added (3.673 g). Subsequently, the solution was transferred into the 800 mL Teflon-lined steel autoclave, sealed, and heated at 120 °C for 24 h. The resulting light blue precipitate was centrifuged and washed with distilled water and ethanol. Lastly, the product was dried for 12 h at 70 °C.

1.4. Physicochemical characterization of materials

1.4.1. Powder X-ray Diffraction (XRD)

X-ray diffraction experiments were carried out using a D8 Advance Diffractometer (Bruker) with the copper Kα1 radiation (λ = 1.5406 Å). The XRD patterns were made in the angular range of 6-50° in 2θ, using a 0.05 ° step size.

1.4.2. Scanning electron microscopy (SEM)

The morphological forms of Cu-MOFs were determined by scanning electron microscope FEI Helios NanoLab 660 equipped with secondary electron detectors: the Everhart-Thornley Detector (ETD) and Through-Lens Detector (TLD). Before measurements, sample preparation was performed by drying ethanolic dispersions of the respective samples on a carbon film fixed on an aluminum sample holder under air. The measurements were carried out in the high-vacuum

mode of 7×10^{-4} Pa at room temperature, both in field-free (FF) and high-resolution (HR) modes. The acceleration voltage was 10 kV, whereas the beam current was 0.2 nA.

1.4.3. Dynamic light scattering (DLS)

The size of MOFs' particles was determined via hydrodynamic diameter analyses using DLS with the Zetasizer Nano ZS (Malvern). Before the measurement, materials were dispersed in water–ethanol solution (1:1) and sonicated for 15 minutes. The analyses were performed for a sample solution of 50 µL at 25 °C, taking an average of 3 measurements per sample.

1.4.4. Low-temperature nitrogen sorption

The textural parameters of Cu-MOF materials were determined by nitrogen adsorption at -196 °C, using the Quantachrome Autosorb IQ apparatus. Before the measurement, samples were degassed for 12 h at 250 °C. The specific surface areas of Cu-BDC and HKUST-1 were calculated with the use of the Brunauer-Emmett-Teller (BET) method, while pore size was evaluated utilizing the Barret-Joyner-Halenda (BJH) method. The micropore surface areas and volume were determined via the t-plot method.

1.4.5. Thermogravimetric analysis (TGA)

Thermogravimetric analysis was performed with the use of the Setsys 1200 apparatus (Setaram). In the measurement, MOF powder (approximately 12–17 mg) was heated from 30 °C to 900 °C at a constant rate of 10 °C/min under nitrogen flow.

1.4.6. Fourier-transform infrared spectroscopy (FT-IR)

The Fourier-transform infrared spectra were registered by using FT-IR Bruker IFS 66v/S spectrometer. The Cu-MOF samples, pure HCQ, and Cu-MOF/HCQ systems (1 mg) were grounded with anhydrous KBr (200 mg), followed by tablet formation. The analysis was conducted in a wavenumber range of 4000–400 cm^{-1} (resolution of 0.5 cm^{-1}; the number of scans: 64).

1.4.7. Zeta potential

Electrokinetic studies were performed to assess the surface charge of HKUST-1 and Cu-BDC materials. Their zeta potential was established as a function of pH by dispersing 10 mg of sample in various buffer solutions (10 mL) of pH 1.2, 4.0, 6.8, 7.2, and 9.0. Subsequently, the measurements were carried out using the Zeta Nano ZS instrument (Malvern Instruments Ltd.).

1.4.8. Cytotoxicity studies

1.4.8.1. Cell culture

hACE2 cells (human ACE2 expressing Hek293 cells) were purchased from InvivoGen (cat. code hkb-hace2). hACE2 are Hek293 cells (human embryonic kidney 293) derived cell lines specifically

generated/engineered for SARS-CoV-2 studies. hACE2 cells stably express human ACE2 (human angiotensin converting enzyme 2) and TMPRSS2 receptors, the host receptors for SARS-CoV-2. Thus, these hACE2 cells are permissive to SARS-CoV-2 Spike pseudotyped lentiviral particles and were used as representative cells for the study. hACE2 cells were maintained and routinely passaged according to the manufacturer's protocol. hACE2 cells were grown as a monolayer in Dulbecco's Modified Eagle's medium (DMEM) (Gibco) containing 4.5 g/L glucose, 2 mM L-glutamine, 10% (v/v) heat-inactivated fetal bovine serum (FBS), 100 U/mL penicillin, 100 µg/mL streptomycin and 100 µg/mL Normocin™ at 37 °C in a humidified atmosphere of 5% CO_2.

1.4.8.2. Cell viability analysis

The effect of HKUST-1 and Cu-BDC on the cell viability was analyzed using the WST-1 colorimetric assay (WST-1 Assay Kit, Abcam). The test is based on the conversion of tetrazolium dye (WST-1) into a colored formazan product by viable, metabolomic active cells. hACE2 were counted using a hemocytometer (Neubauer, Merck) and then seeded in a 96-well sterile culture microplate (Nest Biotechnology Co.) at a concentration of 2 x 10^4 per well. The cells were cultured for 48–72 h to allow the cells to attach and spread on the plate surface. After incubation, when the culture reached near 80% confluence, the medium was removed, and HKUST-1 and Cu-BDC dispersed in the culture medium were added for 24 h. HKUST-1 and Cu-BDC were dispersed in DMEM in the ultrasonic water bath (Elma GmbH & Co KG; 37 kHz, 100% for the setting of the ultrasonic power, sweep mode) before adding to the cells. hACE2 cells were treated with different concentrations of HKUST-1 and Cu-BDC (2 µg/mL, 5 µg/mL, 10 µg/mL, 50 µg/mL, 100 µg/mL). hACE2 cells cultured without HKUST-1 and Cu-BDC served as the control. After 24 h of incubation, WST-1 solution was added to each well (10 µl/ well) and incubated with cells for another 1.5 h in an incubator at 37 °C. The absorbance was determined at 450 nm using a microplate reading spectrophotometer (BioTek). All experiments were performed at least three times. Experimental groups were statistically compared to control group. Statistical significance was calculated using GraphPad Prism, version 6, software, and an unpaired *t*-test.

1.5. Adsorption of HCQ

The synthesized Cu-MOFs were applied as carriers for HCQ, therefore the process of the drug adsorption was performed. At first, the specific amount (25 mg) of each Cu-MOF (HKUST-1 and Cu-BDC) was dispersed in HCQ solutions of the concentration range 2–280 mg/L. Subsequently, the dispersions were agitated at room temperature for 1 h in the temperature-controlled orbital shaker (KS 4000i control, IKA Germany). Then, MOF carriers with adsorbed HCQ were separated *via* centrifugation, and the absorbance of the remaining solutions was measured using Agilent Cary 60 UV-Vis spectrophotometer at a wavelength of 231 nm.

To determine the amount of HCQ adsorbed on each Cu-MOF following formula was applied:

$$q_e = \frac{(C_0 - C_e) \cdot V}{m} \quad (1)$$

where:

C_0 – initial concentration of HCQ solution (mg/L);

C_e – the concentration of HCQ solution (mg/L) remaining after the adsorption process;

V – the volume of the HCQ solution (L);

m – the mass of the Cu-MOF carrier (g).

The obtained adsorption results were analyzed and fitted to two types of adsorption isotherms: Langmuir and Freundlich.[1,2] By referring to the correlation coefficients (R^2) of the models, the mechanism of adsorption has been established.

The Langmuir isotherm is described by the following equation:

$$\frac{C_e}{q_e} = \frac{1}{q_m K_L} + \frac{C_e}{q_m} \quad (2)$$

q_m – the maximum monolayer adsorption capacity of Cu-MOF carrier (mg/g);

K_L – Langmuir constant denoted the energy of adsorption and affinity of binding sites (L/mg).

The Freundlich isotherm is described by the equation (3):

$$\ln q_e = \ln K_f + \frac{1}{n} \ln C_e \quad (3)$$

K_F – Freundlich constant, which relates to the adsorption capacity of the Cu-MOF carrier (mg/g(L $mg^{-1})^{1/n}$);

n – constant, which indicates how favorable is the adsorption process.

1.6. The release studies

1.6.1. The release of HCQ

The release experiments of HCQ from Cu-MOFs were performed in simulated gastric fluid (pH 1.2), intestinal fluid (phosphate buffer of pH 6.8), and saliva (phosphate buffer of pH 7.2). The receptor fluids were maintained at 37.0 °C ± 0.5 °C and stirred at a speed of 200 rpm. Before the release test, 25 mg of Cu-MOF was added to the HCQ solution (5 mg of HCQ in 3 mL of distilled

water) and agitated for 1 h. Then, the mixture was placed in a drier for 12 h at 70 °C. After the solvent evaporation, Cu-MOF/HCQ systems (*i.e.,* HKUST-1/HCQ and Cu-BDC/HCQ) were placed in the dialysis tubing cellulose membrane filled with 3 mL of receptor fluid, sealed, and immersed in the medium (197 mL) of different pH. At specified time intervals, the samples were withdrawn, and the changes in concentration of HCQ were monitored at the wavelength of 231 nm by UV-Vis spectrophotometer (Cary 60, Agilent, U.S.). The data obtained were then used to quantify the percent of HCQ release versus time.

To establish the type of HCQ liberation, datasets were correlated to seven mathematical models: zero-order (% HCQ release vs. time) (eq. 4), first-order (log of % HCQ release vs. time) (eq. 5), Higuchi's model (% HCQ release vs. square root of time) (eq. 6), Hixson-Crowell (cube root of % HCQ remaining vs. time) (eq. 7), Korsmeyer-Peppas model (log of % HCQ vs. log time) (eq. 8), Hopfenberg model ($C_0a_0(1-(1-M_t/M_\infty)^{1/n})$ vs. time) (eq. 9), and Weibull model ($\log(-\ln(1-M_t/M_\infty))$ vs. log of time) (eq. 10).[3,4] M_t is the amount of drug dissolved in time t, and M_∞ is the total amount of drug dissolved. In the Hopfenberg model, C_0 is the initial concentration of the drug in the carrier, and a_0 is the initial radius for a sphere, cylinder, or the half-thickness of a slab. For HKUST-1, it was presumed that a_0 = 40 nm, whilst for Cu-BDC, a_0 = 25 nm. It was also established that HKUST-1 particles are spherical (n_H = 3), and Cu-BDC particles are cylindrical (n_H = 2). In the Weibull model, a simplified equation has been used (10), which included the release curve in the exponential form (b = 1). For all models, the criterion of fitting was the correlation coefficient (R^2), whose highest value indicated the most probable release mechanism.[5]

$$F_t = k_0 t_e \quad (4)$$

$$F_t = 1 - e^{-kt} \quad (5)$$

$$F_t = k_H \sqrt{t} \quad (6)$$

$$\sqrt[3]{F_0} - \sqrt[3]{F_t} = k_{HC} t \quad (7)$$

$$F_t = k_{KP} t^{n_{KP}} \quad (8)$$

$$F_t = 1 - (1 - \left(\frac{k_H t}{C_0 a_0}\right)^{n_H}) \quad (9)$$

$$F_t = 1 - e^{-k_W (t-T)} \quad (10)$$

F_t – the fraction of HCQ released in time;

F_0 – the initial amount of HCQ in the nanocarrier;

k_0, k_t, k_H, k_{HC}, k_{KP}, k_H, k_w – the release constants of particular kinetic models;

t – time of the release;

T – the latency time of the release process;

n_{KP} – the diffusion exponent;

n_H – value corresponds to the geometrical form of carrier particles, 1 for the film, 2 for the cylinder, and 3 for the sphere.

1.6.2. The release of Cu^{2+}

The release of Cu^{2+} from HKUST-1 and Cu-BDC materials was performed in simulated gastric fluid (pH 1.2), intestinal fluid (phosphate buffer of pH 6.8), and saliva (phosphate buffer pH 7.2) at 37.0 °C ± 0.5 °C. 50 mg of each sample was dispersed in 200 mL of medium. At a certain period (after 10 min, 30 min, 1 h, 2 h, 4 h, and 8 h), 1 mL of the solution was taken for analysis and replaced by 1 mL of a fresh receptor fluid. The amount of Cu^{2+} in the 1 mL sample was determined by inductively excited plasma mass spectrometer ICP-MS NexION 300d (Perkin Elmer). The copper ions-release studies were done in triplicates, and data are presented as mean ± standard deviation.

1.7. Antiviral activity

1.7.1. Pseudovirons (PsVs) production

SARS-CoV-2 PsVs were generated using pPACK-SPIKE SARS-CoV-2 "S" Pseudotype Lentivector Packaging System (SBI, System BioSciences). Briefly, HEK293TT were transfected with the pPACK-SPIKE Packaging Mix consisting of three plasmids producing the structural and replication proteins needed to generate "Spike" pseudotyped lentiviral particles along with the luciferase reporter plasmid pLL-CMV-Luciferase-T2A-Puro (SBI, System BioSciences). Similarly, pPACK-SPIKE SARS-CoV-2 "S" Pdeudotype Lentivector Packing System with the pCDH-CMV-MCS-EF1-copGFP lentivector (System BioSciences, SBI) was used to preparation of SARS-CoV-2 PsVs carrying a GFP (green fluorescent protein) reporter vector. At 72 h after transfection, the cell medium was collected, and pPACK SPIKE pseudovirions containing luciferase or GFP reporter plasmid were concentrated using PEG-it solution and following the manufacturer's instructions. Purity and capsid protein content was determined by SDS-PAGE and Coomassie brilliant blue staining. The pseudoviral titer was determined by Real-Time PCR, and the copy number was quantified using a standard curve of reporter plasmid DNA.

1.7.2. Infectivity assay

hACE2 cells were seeded in 96-well plates at a density of 2 x 10^4 cells/well. After 48 h, cells were first treated with non-toxic concentrations of HKUST-1 and Cu-BDC for 3 h and then exposed to 1 vge/cell of SARS CoV-2 luciferase reporter-positive PsVs. Infection was monitored after 30 h by luminometric analysis of firefly luciferase activity using the Luciferase Assay System (Promega). The infection was normalized to 100% as the value obtained with untreated cells, and this was used to calculate the percentage reduction following treatment of the cells with HKUST-1, Cu-BDC, and Cu-MOF/drug systems, *i.e.,* HKUST-1/HCQ and Cu-BDC/HCQ. Equal amounts of total cell

protein extract were used in the luciferase measurements. All experiments were performed at least three times. Experimental groups were statistically compared to control group. Statistical significance was calculated using GraphPad Prism, version 6, software, and an unpaired *t*-test.

1.7.3. Visualization of SARS-CoV-2 infection/Live Imaging In Vitro

In order to visualize infection of hACE2 cells, produced SARS-CoV-2 PsVs with a GFP-reported gene were used. hACE2 cells were seeded in 8-well LabTek Chambered Coverglasses System (Nunc) at a density of 3 x 10^4 cells/well and incubated at 37 °C in a humidified atmosphere of 5% CO_2. After 48 h, the cells were exposed to 10 vge/cell of SARS CoV-2 GFP reporter-positive PsVs. Then, 26 h after infection, hACE2 cells were observed in Living Cell Fluorescence Imaging Medium (FluoroBrite™ DMEM, Gibco) using a confocal microscope (Zeiss) with a 40x objective. 488 nm laser was used for fluorescence excitation of the GFP and SARS-CoV-2 PsVs were detected via their fluorescence (green). The images were analyzed with ZEN 3.5 (Zeiss).

1.7.4. Enzyme-Linked Immunosorbent Assay (ELISA)

In order to verify further if HKUST-1 and Cu-BDC carriers (pristine and HCQ-loaded) can inhibit the interaction between SARS-CoV-2 Spike protein and ACE2 receptor, the colorimetric ELISA assay was applied following described protocol (SARS-CoV-2 Spike–ACE2 Binding Inhibitor Screening Fast Kit, EpigenTek Group Inc.). In the procedure, the microplate wells pre-coated with SARS-CoV-2 Spike protein were used. His-tagged ACE2 was bound to the coated Spike protein in the presence or absence of samples, which were tested at the same concentration as in the infection assay. The amount of the bound ACE2, which is proportional to ACE2 inhibition intensity, was then recognized by the Binding Detection Solution containing anti-His antibody. It was assessed through an ELISA-like reaction via absorbance measurement in the microplate spectrophotometer (Synergy H1 Hybrid Reader, BioTek Instruments, Inc.) at a wavelength of 450 nm (Scheme 1).

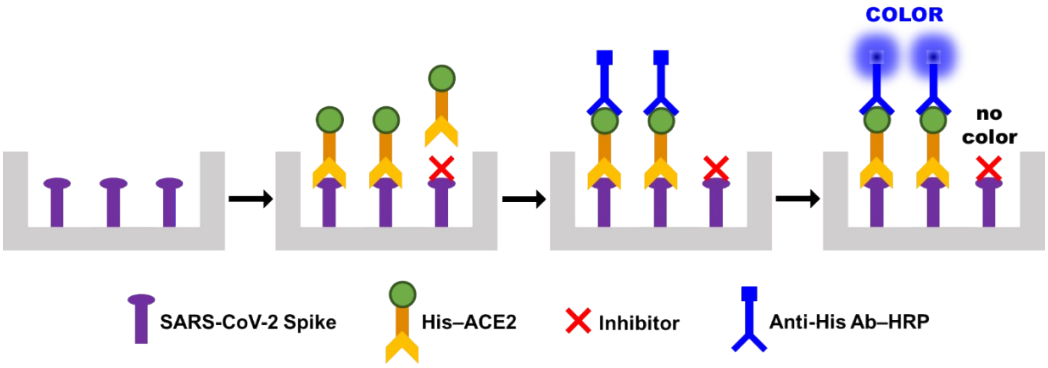

Scheme S1. The procedure of the SARS-CoV-2 Spike – ACE2 Binding Inhibitor Screening Fast Kit.

2. Supplementary Figures and Tables

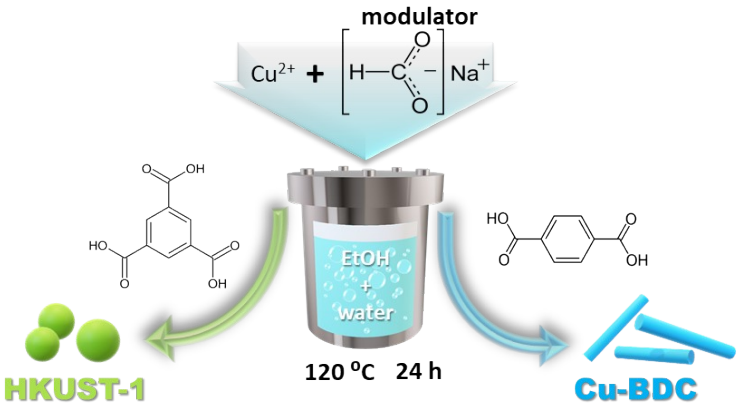

Figure S1. Illustration of solvothermal synthesis of nanosized Cu-MOFs: spherical HKUST-1 and cylindrical Cu-BDC.

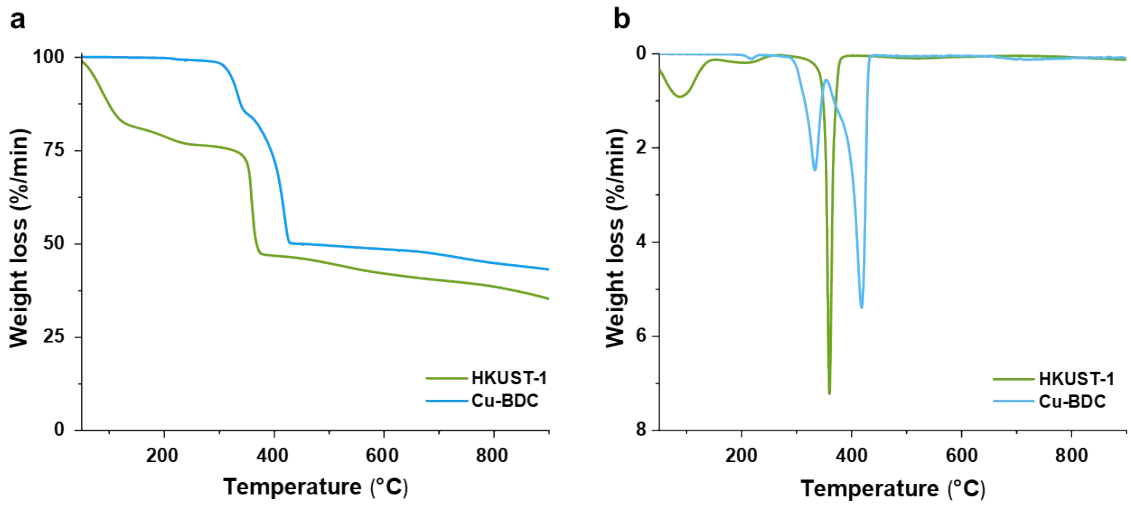

Figure S2. Thermogravimetric analysis (a – TG, b – DTG curves) of HKUST-1 and Cu-BDC.

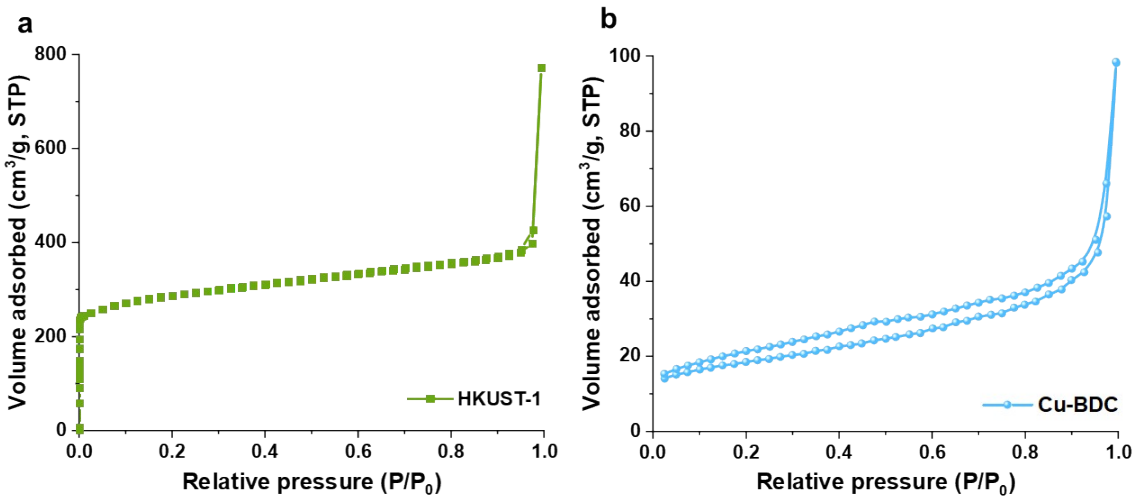

Figure S3. N_2 adsorption/desorption isotherms of (a) HKUST-1 and (b) Cu-BDC.

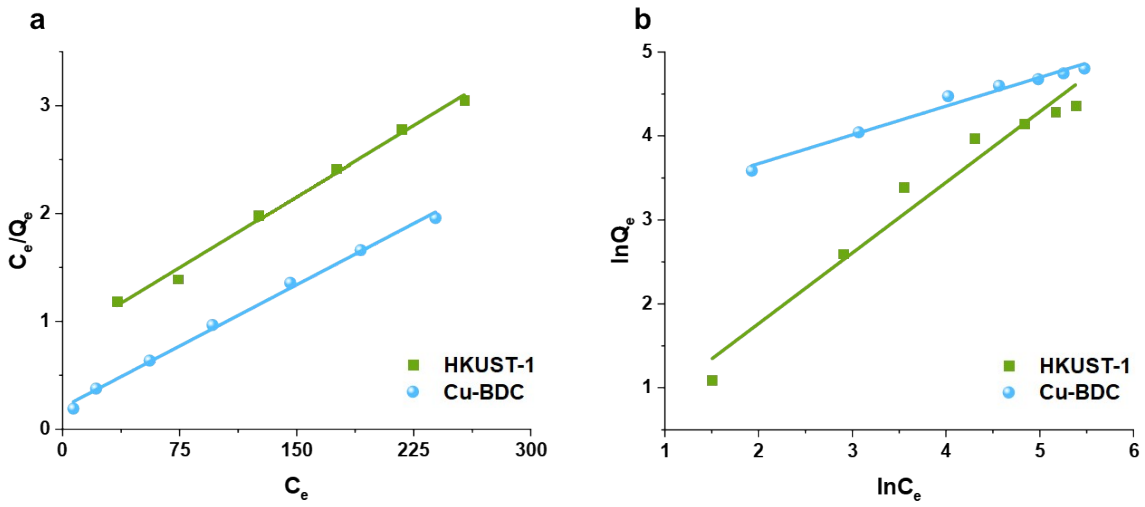

Figure S4. The fit of experimental HCQ adsorption data to linear forms of Langmuir (a) and Freundlich (b) isotherm models.

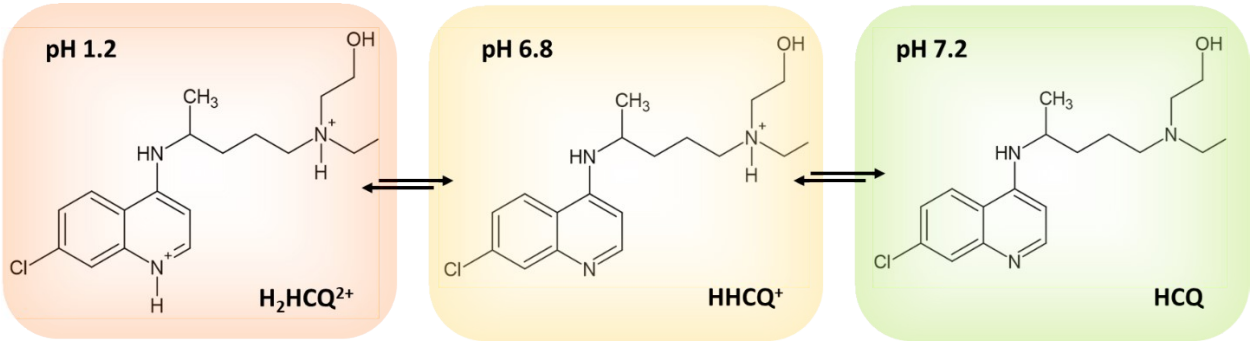

Figure S5. Dissociation equilibrium of HCQ and occurrence of a predominant form at a various pH (1.2, 6.8, and 7.2). H_2HCQ^{2+} and $HHCQ^{+}$ stand for diprotonated and monoprotonated HCQ, respectively.

HCQ is a weak base, which has three basic functional groups with the following pKa: 4.00, 8.27, and 9.67. In a strongly acidic environment ($pH \leqslant 4$), it is fully protonated (H_2HCQ^{2+}). However, at pH 7, it exits in diprotonated (H_2HCQ^{2+}; ~66%) and monoprotonated forms ($HHCQ^{+}$; ~34%). Moving towards more alkaline solutions, there is a percentage increase in monoprotonated forms. Under strongly alkaline conditions, the drug is present in an uncharged form.[6] Due to the fact that the HCQ release processes were carried out in the receptor fluids of pH 1.2, 6.8, and 7.2, the drug forms for selected conditions are presented.

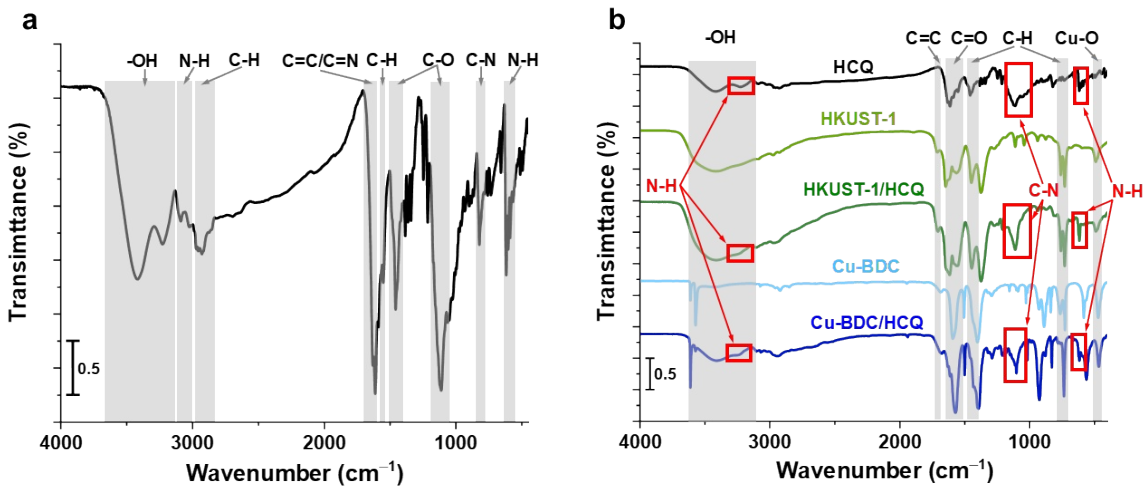

Figure S6. FT-IR spectra of (a) HCQ; (b) pristine Cu-MOFs, and Cu-MOF/HCQ delivery systems.

The FT-IR analysis of the pure HCQ (Fig. S6 a) revealed the following bands of main functional groups. At the wavenumber of 628 cm^{-1} and 3038 cm^{-1}, the bands of N–H were noted. The lower range band corresponds to the N–H bending vibrations, while the higher range can be assigned to the N–H axial deformations. In addition, at ~3000 cm^{-1}, there is a weak band, which is typical for secondary or tertiary amines. The band detected at 820 cm^{-1} is a confirmation of C–N stretching vibrations. In contrast, the double bonds of C=N in the aromatic ring that are present in the HCQ structure can be seen as an overlapping band at the 1603–1611 cm^{-1} range. The signal in this area also corresponds to the aromatic C=C bonds. The presence of aryl C–H can be detected at 1550 cm^{-1}, whereas those belonging to the aliphatic chain resulted in a small band in the 2850–3018 cm^{-1} range. At the wavenumber of 1106 cm^{-1} and 1453 cm^{-1}, axial vibrations of C–O bonds are noticeable. In the range of 3670–3125 cm^{-1}, there is a typical wide band, which is assigned to the axial deformation of the alcohol (–OH) and/or the presence of water in the HCQ.[6,7] The pristine Cu-MOFs show similar broad bands in this range differing in intensity, typical of hydroxyl groups and water. The two distinctive sharp bands at 3571 cm^{-1} and 3611 cm^{-1} registered for Cu-BDC were previously recorded,[8] and they can be attributed to hydrogen bonds.[9] HKUST-1 and Cu-BDC indicated the same band at 1109 cm^{-1} assigned to C–O–Cu stretching vibrations.[10] Bands in the ranges of 1660–1500 cm^{-1} and 1460–1330 cm^{-1} correspond to asymmetric and symmetric stretching vibrations of carboxylic groups.[11] In the FT-IR spectra of HKUST-1/HCQ and Cu-BDC/HCQ delivery systems (Fig. S6 b), the bands at 1550 cm^{-1} and 1650 cm^{-1} can be assigned to the stretching vibrations of C=O and C=C, respectively. Moreover, multiple C–H vibrations from phenyl rings are noted at ~740 cm^{-1} and ~1500 cm^{-1}.[12] These bands are slightly shifted in comparison to FT-IR spectra of Cu-MOF nanocarriers proving the π-π interactions with drug. The presence of the drug anchored to the Cu-MOF nanoparticles can be revealed by appearing new bands at the wavenumber in the range of 3100–3300 cm^{-1} primarily derived from hydrogen bonds between carboxylic groups of samples and the nitrogen present in the drug. Furthermore, the

band at 1200 cm^{-1} is typical for bending C–N vibrations, and a small band at 630 cm^{-1} attributed to wagging vibrations of N–H are well visible.[6]

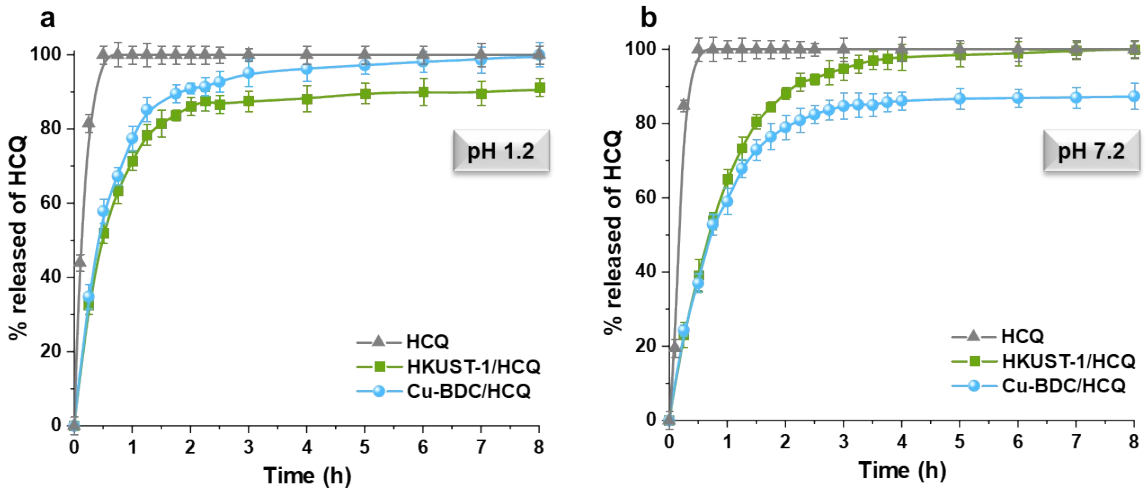

Figure S7. Release profiles of HCQ from HKUST-1 and Cu-BDC and dissolution rate of pure HCQ at pH 1.2 (a) and 7.2 (b).

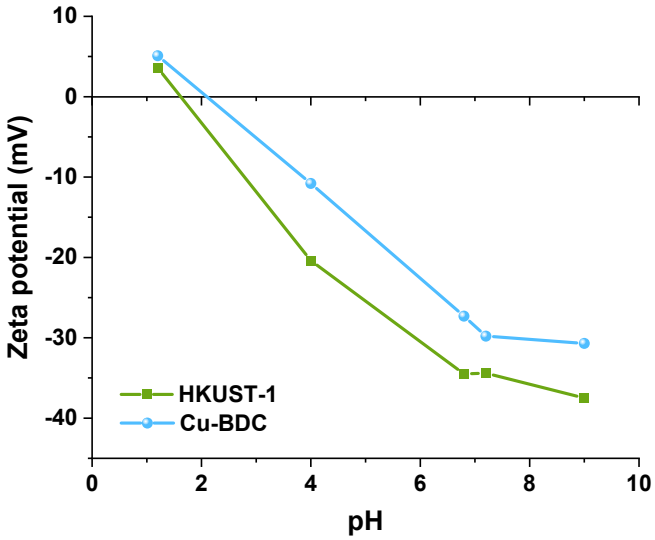

Figure S8. Change of zeta potential of HKUST-1 and Cu-BDC materials as a function of pH.

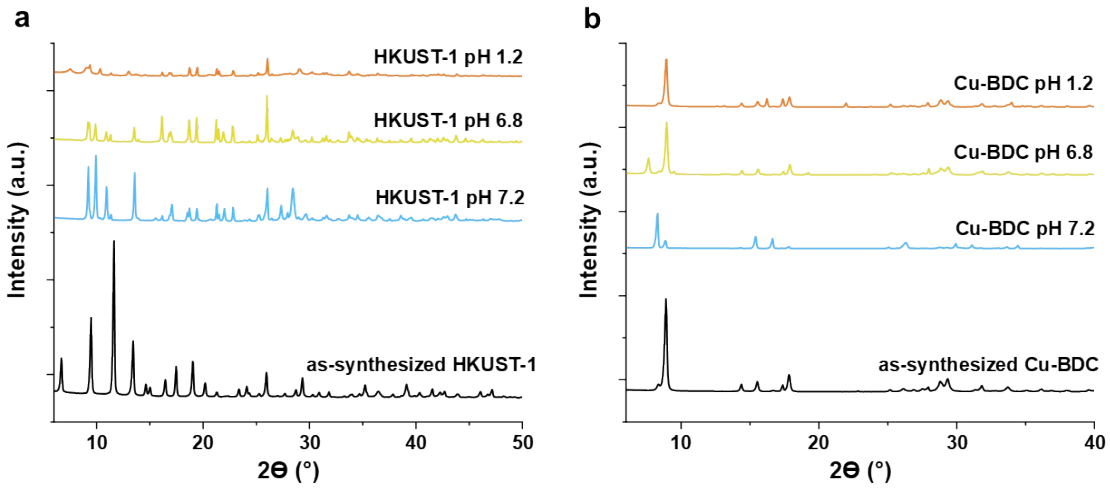

Figure S9. XRD profiles of HKUST-1 (a) and Cu-BDC (b).

In order to test the stability of HKUST-1 and Cu-BDC carriers, the XRD analysis was performed after their agitation for 8 h in the receptor fluids of pH 7.2, 6.8, and 1.2. XRD profiles of Cu-MOFs indicated their framework is responsive to the pH change of medium. For HKUST-1 the positions and intensity of the reflections altered as the pH decreased. This can be the result of Cu–O bond disruption in the outer layers of MOF by ligand displacement with water substitution,[13] followed by ligand detachment.[14–16] In the solutions with pH of 7.2 and 6.8, it can be assumed that copper-oxo species and isolated linkers with partially coordinated positions are still present in the material.[17] After immersing in the medium of pH 1.2, there was a significant disappearance of reflections from HKUST-1, signalling a complete loss of its crystalline phase. In contrast, the Cu-BDC demonstrated higher stability at applied conditions, however, phase transition was noted. Residual solvents taken for synthesis (water and ethanol) may have been present in the pristine material. The change in the position of the Cu-BDC reflections after agitation in the receptor fluids of pH 7.2, 6.8, and 1.2 can be caused by the replacement of the coordinated solvent mixture with water, forming Co(BDC)$(H_2O)_2$.[18,19]

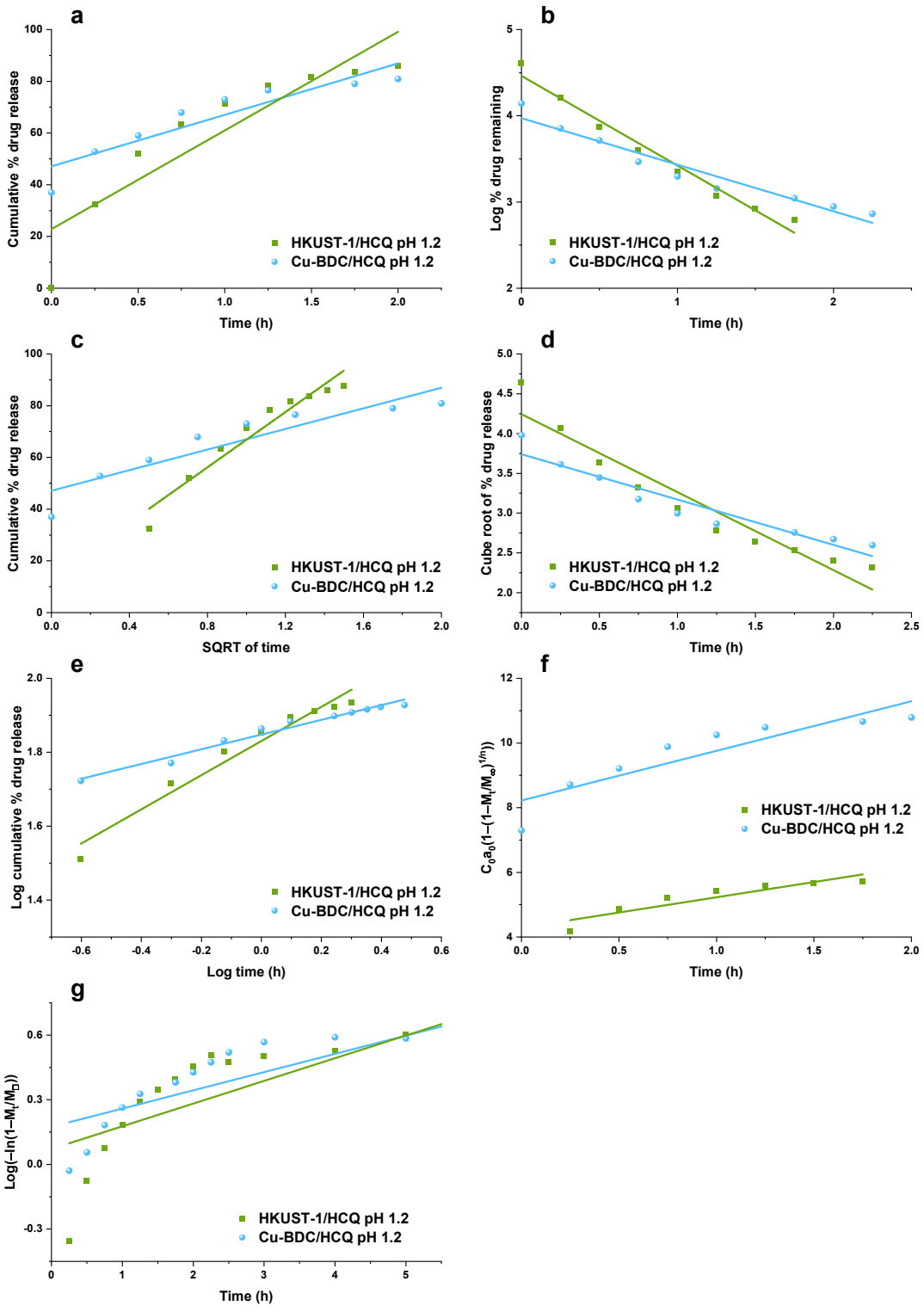

Figure S10. The release data of HCQ from HKUST-1 and Cu-BDC in the simulated gastric fluid of pH 1.2, fitted to various kinetic models: (a) zero-order model; (b) first-order model; (c) Higuchi model; (d) Hixson-Crowell model; (e) Korsmeyer-Peppas model; (f) Hopfenberg model; and (g) Weibull model.

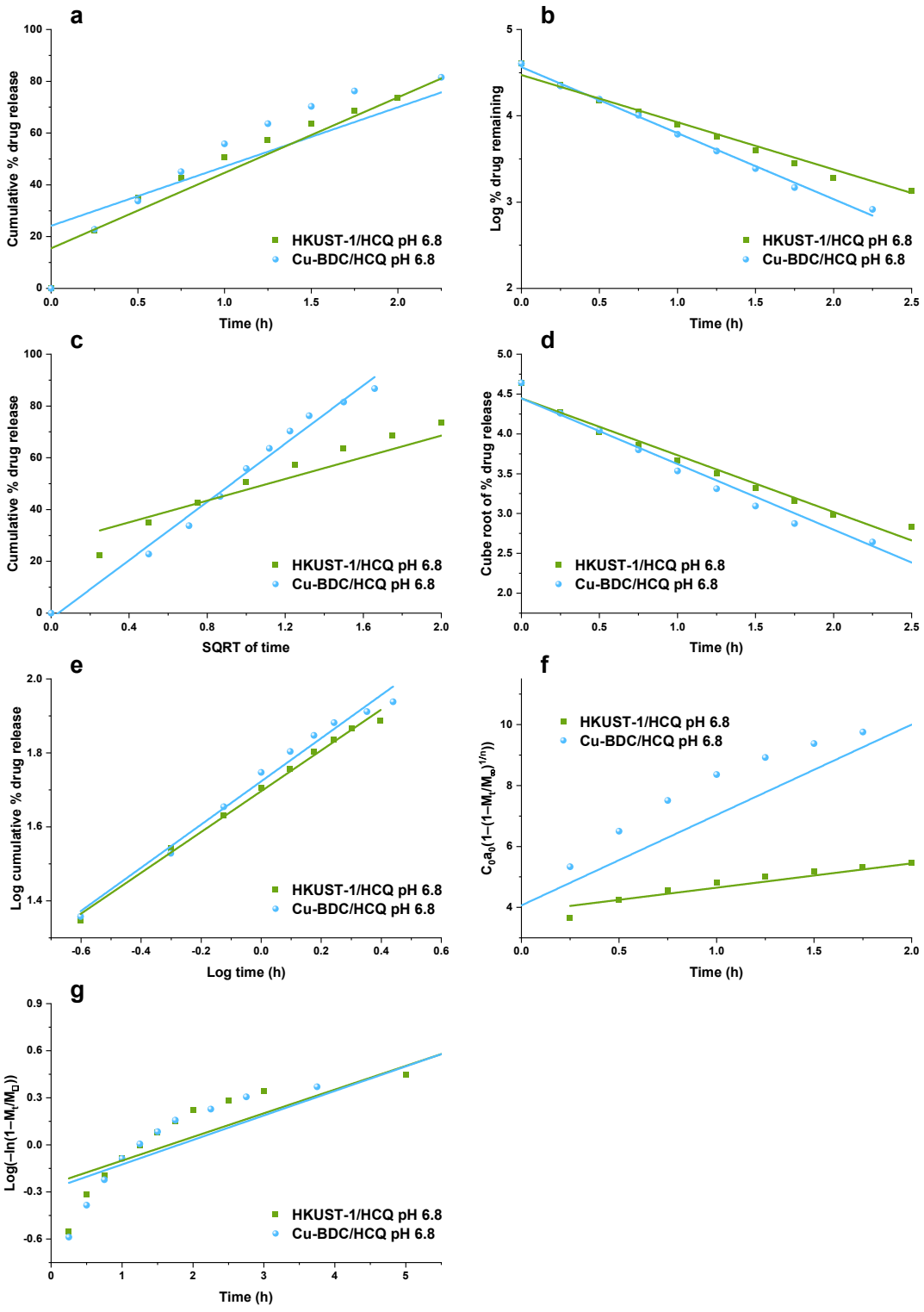

Figure S11. The release data of HCQ from HKUST-1 and Cu-BDC in the phosphate buffer of pH 6.8, fitted to various kinetic models: (a) zero-order model; (b) first-order model; (c) Higuchi model; (d) Hixson-Crowell model; (e) Korsmeyer-Peppas model; (f) Hopfenberg model; and (g) Weibull model.

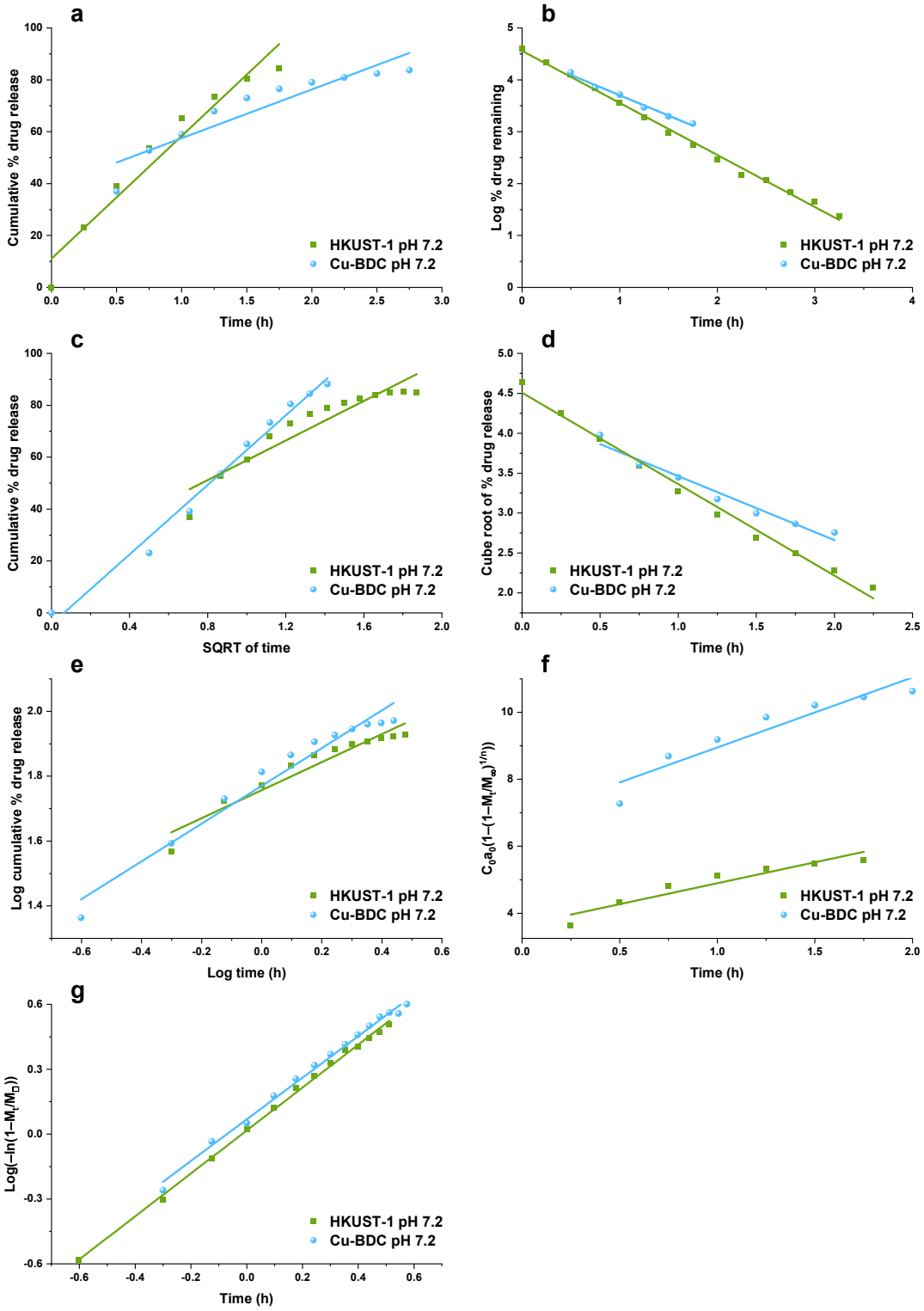

Figure S12. The release data of HCQ from HKUST-1 and Cu-BDC in the phosphate buffer of pH 7.2, fitted to various kinetic models: (a) zero-order model; (b) first-order model; (c) Higuchi model; (d) Hixson-Crowell model; (e) Korsmeyer-Peppas model; (f) Hopfenberg model; and (g) Weibull model.

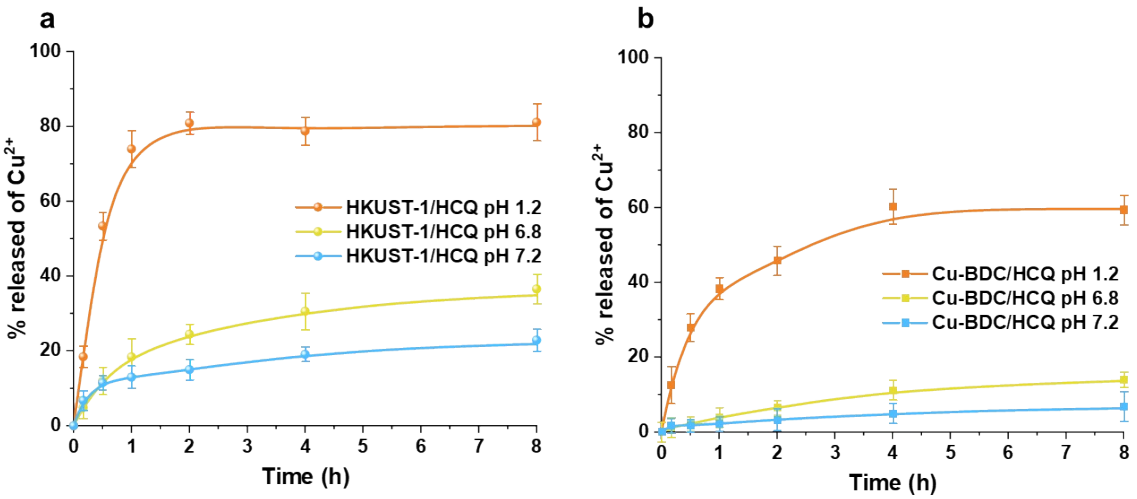

Figure S13. Release profiles of Cu^{2+} from HKUST-1 (a) and Cu-BDC (b) at pH 1.2, 6.8, and 7.2.

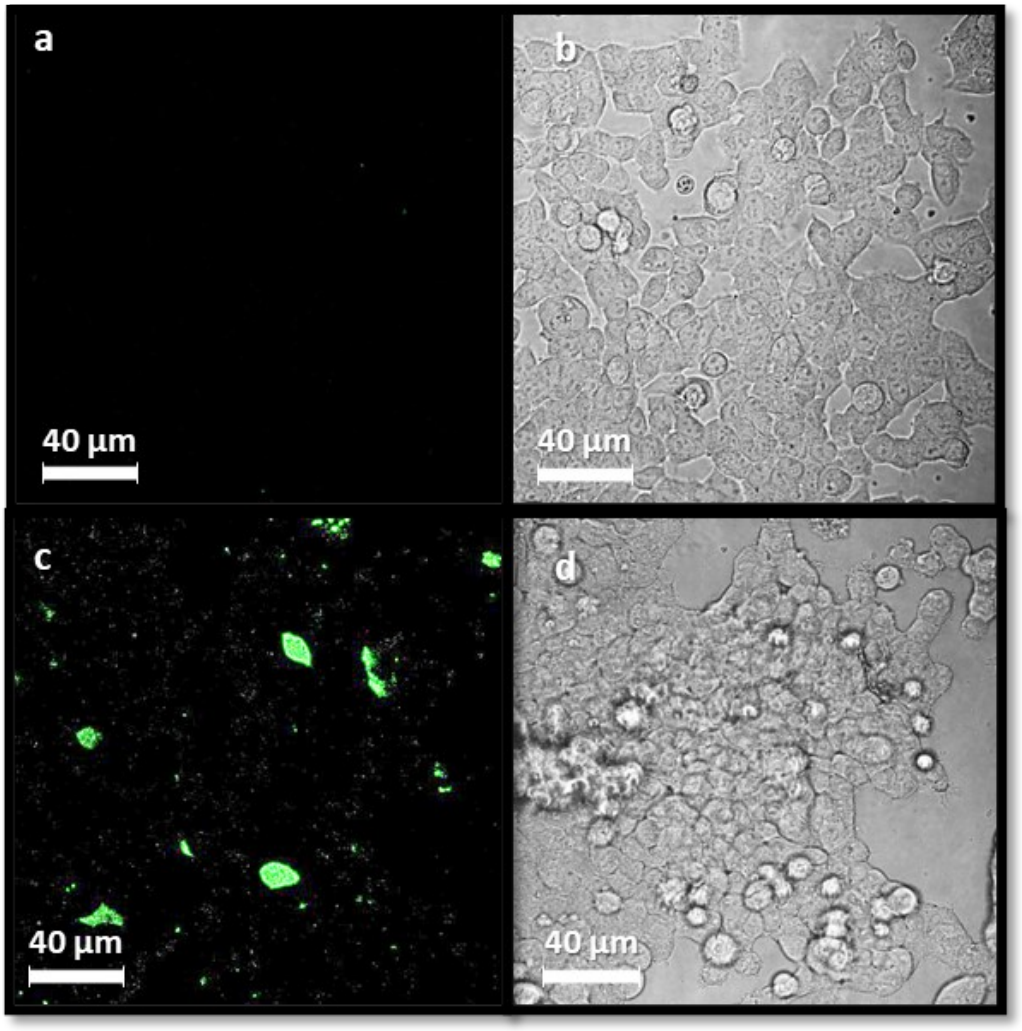

Figure S14. Confocal microscopy images of hACE2 cells: (a, b) non-infected, (d, c) exposed to SARS-CoV-2 PsVs (green fluorescence).

Table S1. Textural parameters of Cu-MOFs calculated from the N_2 adsorption isotherms.

Sample	BET surface area (m^2/g)	Micropore area (m^2/g)	Total pore volume (cm^3/g)	Micropore volume (cm^3/g)
HKUST-1	979	859	1.20	0.42
Cu-BDC	62	26	0.15	0.02

Table S2. The parameters calculated from fitting the results of the adsorption isotherms of HCQ onto HKUST-1 and Cu-BDC materials to the Langmuir and Freundlich models.

Material	Langmuir			Freundlich		
	Q_m (mg/g)	K_L (L/mg)	R^2	K_f (mg/g(L/mg)$^{1/n}$)	1/n	R^2
HKUST-1	114	0.011	0.994	1.09	0.841	0.974
Cu-BDC	132	0.038	0.996	19.80	0.342	0.980

Table S3. Kinetic models applied to describe the release mechanism of HCQ from HKUST-1 and Cu-BDC at pH 1.2, 6.8, and 7.2.

Material	Zero-order		First-order		Higuchi		Hixson-Crowell		Korsmeyer-Peppas			Hopfenberg		Weibull	
	R^2	k_0	R^2	k_1	R^2	k_H	R^2	k_{HC}	R^2	k_{KP}	n_{KP}	R^2	k_H	R^2	k_W
								pH 1.2							
HKUST-1	0.827	38.158	0.977	1.040	0.937	53.468	0.922	0.980	0.962	67.679	0.462	0.845	0.943	0.934	0.667
Cu-BDC	0.850	19.910	0.940	0.540	0.979	32.493	0.912	0.570	0.973	70.447	0.200	0.815	1.535	0.978	0.529
								pH 6.8							
HKUST-1	0.907	29.157	0.979	0.547	0.980	49.246	0.970	0.713	0.994	49.720	0.552	0.891	0.798	0.986	0.777
Cu-BDC	0.813	22.890	0.995	0.765	0.987	56.255	0.974	0.824	0.985	52.854	0.583	0.695	2.968	0.984	0.856
								pH 7.2							
HKUST-1	0.945	47.267	0.996	1.003	0.987	66.982	0.990	1.145	0.963	58.900	0.582	0.904	1.250	0.990	0.993
Cu-BDC	0.866	18.772	0.988	0.783	0.955	54.091	0.969	0.801	0.955	57.416	0.504	0.896	2.090	0.981	0.962

References

1 I. Langmuir, *J. Am. Chem. Soc.*, 1918, **40**, 1361–1403.

2 F. H. M. F., *J. Phys. chem.*, 1906, **57**, 1100–1107.

3 S. Dash, P. N. Murthy, L. Nath and P. Chowdhury, *Acta Pol. Pharm. - Drug Res.*, 2010, **67**, 217–223.

4 M. L. B. T.-S. to M. the D. R. from P. S. Bruschi, Ed., in *Strategies to Modify the Drug Release from Pharmaceutical Systems*, Woodhead Publishing, 2015, pp. 63–86.

5 Ramteke K.H., *Sch. Acad. J. PharmacyOnline) Sch. Acad. J. Pharm*, 2014, **3**, 388–396.

6 A. Olejnik and J. Goscianska, *Mater. Sci. Eng. C*, 2021, **130**, 112438.

7 A. N. F. Moraes, L. A. D. Silva, M. A. de Oliveira, E. M. de Oliveira, T. L. Nascimento, E. M. Lima, I. M. S. Torres and D. G. A. Diniz, *J. Therm. Anal. Calorim.*, 2020, **140**, 2283–2292.

8 R. S. Salama, S. E. Samra, A. I. Ahmed, S. A. El-Hakam, S. E. Samra and S. M. El-Dafrawy, *Int. J. Mod. Chem.*, 2018, **10**, 195–207.

9 M. R. Lacroix, X. Gao, Y. Liu and S. H. Strauss, *J. Fluor. Chem.*, 2019, **217**, 105–108.

10 G. Zhan, L. Fan, F. Zhao, Z. Huang, B. Chen, X. Yang and S. Zhou, *Adv. Funct. Mater.*, 2019, **29**, 1806720.

11 F. S. Gentile, M. Pannico, M. Causà, G. Mensitieri, G. Di Palma, G. Scherillo and P. Musto, *J. Mater. Chem. A*, 2020, **8**, 10796–10812.

12 A. H. Khoshakhlagh, F. Golbabaei, M. Beygzadeh, F. Carrasco-Marín and S. J. Shahtaheri, *RSC Adv.*, 2020, **10**, 35582–35596.

13 X. Ma, L. Wang, H. Wang, J. Deng, Y. Song, Q. Li, X. Li and A. M. Dietrich, *J. Hazard. Mater.*, 2022, **424**, 126918.

14 J. R. Álvarez, E. Sánchez-González, E. Pérez, E. Schneider-Revueltas, A. Martínez, A. Tejeda-Cruz, A. Islas-Jácome, E. González-Zamora and I. A. Ibarra, *Dalt. Trans.*, 2017, **46**, 9192–9200.

15 W. Xue, Z. Zhang, H. Huang, C. Zhong and D. Mei, *J. Phys. Chem. C*, 2020, **124**, 1991–2001.

16 L. N. McHugh, M. J. McPherson, L. J. McCormick, S. A. Morris, P. S. Wheatley, S. J. Teat, D. McKay, D. M. Dawson, C. E. F. Sansome, S. E. Ashbrook, C. A. Stone, M. W. Smith and R. E. Morris, *Nat. Chem.*, 2018, **10**, 1096–1102.

17 G. Majano, O. Martin, M. Hammes, S. Smeets, C. Baerlocher and J. Pérez-Ramírez, *Adv. Funct. Mater.*, 2014, **24**, 3855–3865.

18 C. G. Carson, K. Hardcastle, J. Schwartz, X. Liu, C. Hoffmann, R. A. Gerhardt and R. Tannenbaum, *Eur. J. Inorg. Chem.*, 2009, 2338–2343.

19 Y. Jing, Y. Yoshida, P. Huang and H. Kitagawa, *Angew. Chemie - Int. Ed.*, 2022, **61**, e202117417.